Preferred citation: A. Sibellas, J.E.Q.M. Litjens, J. Drummond, A.B. Phillion and D.M. Martinez. Visualisation of the 3D microstructure of a monodisperse fibre assembly under uniaxial compression. In *Advances in Pulp and Paper Research*, Cambridge 2022, Trans. of the XVIIth Fund. Res. Symp. Cambridge, 2022 (D. Coffin and W. Batchelor, eds), pp 91–103. FRC, Manchester, 2022. DOI: 10.15376/frc.2022.1.91.

VISUALISATION OF THE 3D MICROSTRUCTURE OF A MONODISPERSE FIBRE ASSEMBLY UNDER UNIAXIAL COMPRESSION

*A. Sibellas[1,] *, J.E.Q.M. Litjens[1], J. Drummond[1], A.B. Phillion[2] and D.M. Martinez[1]*

[1] Department of Chemical and Biological Engineering, The University of British Columbia, Vancouver, Canada
[2] Department of Materials Science and Engineering, McMaster University, Hamilton, Canada

ABSTRACT

In this work we visualize the evolution of the 3D microstructure of a mono-disperse nylon fibre floc undergoing uniaxial compression. In total seven stages of compression were visualized using X-ray micro-computed tomography. We observe that at the early stages of compression, densification occurred through sliding and rotation; at later stages, densification occurred though individual fibre deformation. We quantified these images and estimated the density of inter-particle contacts ρ_c as a function of the compressive strain ε_c and found that $\rho_c \propto \varepsilon_c^3$

* Corresponding author

1 INTRODUCTION

There is a need to characterize the microstructure of fibre assemblies in a manner that gives insight into the macroscopic mechanical behaviour. In this work, we visualize the evolution of the 3D microstructure of a monodisperse nylon fibre floc under uniaxial compression and report the number of contacts per unit volume ρ_c as a function of the load and solid volume fraction φ. Although an extensive theoretical literature exists on the architecture of fibre assemblies [1], the primary focus of our work is to advance visualization tools of samples under mechanical stress, such as those pioneered by Thibault and Bloch [2]. Specifically, we have quantified the evolution of the nylon fibre bundle's architecture under deformation using microtomography. The key technical challenge is the characterization of the inter-particle contact as blurring and noise create experimental artifacts.

Before proceeding, it is instructive to first review the existing methodologies to estimate ρ_c. Particle connectivity in random assemblies has been the subject of diverse theoretical, numerical and experimental investigations and the literature in this area is substantial. We note two commonly used methodologies, destructive and non-destructive, which we describe below. In the first category, the liquid-bridge method [3], introduced in 1929 for granular materials, is perhaps the most widely adopted destructive protocol [4, 5, 6, 7, 8, 9]. Here, porous media are immersed in paints and ρ_c is determined by counting of the unstained regions. Although simple, there is a systematic over approximation of ρ_c when compared to numerical and theoretical works. In the second category, 3D X-ray microtomography is rapidly being adopted as the gold-standard as this methodology allows for a 3D rendering of the local architecture with the potential of segmentation of the individual grains. The key scientific challenge is delineating true from false contacts in these images as artefacts such as blur and noise combined with the partial volume effect create features where close-contacts appear as if the grains are touching [10].

Several methods have been developed to decouple true from false contacts in 3D tomographic images. Wiebicke et al. [10] applied a local threshold on the contact regions between pebbles to arbitrarily lower contact over-detection. Aste et al. [11], for a mono-dispersed packing of spheres, resolved the centroid of each particle and obtained the number of contact per particle from growing virtual spheres. Schaller et al. [12] and Fu et al. [13, 14] then extended Aste's approach to obloïd and rod -shaped objects, respectively. However, this method crucially relies on determining the center-line of the individual object; difficulties also arise when treating end-to-end and end-to-side contacts. More recently, a promising hybrid method for spheres was reported by Delaney et al. [15] by combining the structure obtained by tomography with simulations using a Discrete Element Method (DEM). Good agreement was found between this work and the theory advanced by Song et al. [16].

In a recent study, we proposed a clustering algorithm to segment true from false contacts. Critically, we argued that the contact-area probability distribution is formed by the superposition of two sub-populations, true and false, and performed an *in-situ calibration* of the true-contact-sub-population-distribution through use of physical phantoms, i.e. manufactured-constructs of known size, packing and contact locations which have been imaged. Once calibrated, we were able to reproduce the theoretical findings of Song et al. [16] for both random packed spherical beds and polydispersed geometries.

In this work, we examine the architecture of nylon fibre assemblies, subsequently referred to as flocs. Uniquely, we report on an X-ray tomographic imaging campaign where we recorded the micro-structure of the floc at various levels of compression. Using an *in-situ* compression apparatus we simultaneously measured the stress-strain behaviour of the floc. This resulted in a library of 3D micro-structural images at various degrees of compression that we used to analyze deformation mechanisms. In §2 we report on the characteristics of the floc, the imaging protocols and the image quantification routines. In §3 we display the micro-structural images and report on ρ_c as a function of φ.

2 METHODS AND MATERIALS

In this section we report on the experimental procedure for *in-situ* compression, imaging, and image quantification. We will begin by describing the nylon floc, the imaging protocol and the data-polishing pipeline to create a usable image for quantification. Following this, we report on our image quantification methodology to estimate ρ_c.

To begin, we used a nearly spherical 11 mm diameter commercial nylon floc with an initial volume fraction of $\varphi_o = 0.108$ as determined through gravimetric measurements. The floc was chosen as spherical as possible without any visible sign of preferential orientation of the fibres. It was carefully handled to avoid undergoing mechanical stress. The specific gravity of a nylon fibre was set to 1.1 for this estimation. As shown in Figure 1a, in the uncompressed state the floc forms a static structure which is also (somewhat) elastic. Each fibre in the floc may be approximated as a rod with length 3.2 mm and a diameter of 42 μm measured with a high-resolution flatbed scanner, see Figures. 1b–c. We note some curvature in the fibres in their initial state.

For compression, we used a Deben CT5000 (https://deben.co.uk) with a 5 kN load cell. Compression is achieved by moving the lower platen upwards at a prescribed rate and step size while the upper platen is held stationary. The floc was secured to the lower-platen using two-sided tape; a traction-free condition was imposed on the upper platen. The Deben was operated in displacement-controlled

mode where we measured the resulting force at a frequency of 10 Hz. Two separate experiments were performed. In the first study we compressed a single floc continuously, at a rate of 0.5 mm/min and recorded the resulting force. In the second study, we programmed a series of 1 mm compression steps, at a rate of 0.5 mm/min, and 8 hours hold sequences, which were repeated for a total displacement of 6 mm.

3D X-ray tomographic imaging was performed using a Zeiss Xradia Versa 520 (zeiss.com/microscopy). The *insitu* compression cell was placed in the microscope and its elevation was adjusted so that the field of view was slightly under the top stationary platen, as shown schematically in Figure 1d. More specifically, we adjusted the field of view to be 2 mm, with its centroid located 1.4 mm below the upper platen. With this, the gap between the upper edge of the field of view and the platen was 0.4 mm, representing a distance of approximately 9 fibre diameters. Our field of view remained fixed for all scans. In total we performed 7 scans with identical recipies. We collected 16 bit images of dimensions 1000 x 1000 x 1000 voxels with a resolution of 2 μm. The CCD detector provides 2000 x 2000 pixels but a pixel binning of 2 was used to reduce the overall scanning time to 5 hours. The voltage of the X-ray tube was set to 60 kV (5W), while 3201 projections were acquired during sample rotation of 360° with an exposure time of 5 seconds per projection. Imaging commenced after 3 hours of hold sequence for the stress relaxation to be stabilized.

After acquiring the 3D datasets, each was segmented, denoised, and analyzed in a four step procedure:

(a) Noise was removed from the image using XLib [17] in Fiji, a 3D anisotropic diffusion filter advanced by Tschmperlé and Deriche [18].
(b) Binarization of the grayscale images was then performed using a carefully chosen intensity threshold.
(c) Overlapping or touching objects were separated by first creating a 3D Euclidian distance map (EDM) of the binary image and then applying a watershed segmentation method [19]. These routines was performed in Fiji using the 3D Image Suite plug-in [20]. Seeding prevented oversegmentation, with the seed points found by calculating the extended-maxima of the EDM.
(d) The segmented image was then was subtracted from the binarized image to capture the contact surfaces.

This image analysis pipeline is shown in Figure. 2 for a 2D slice, beginning with the as-acquired data (Figure 2a), followed by denoising (Figure 2b), binarization (Figure 2c), and fibre segmentation (Figure 2d). The resulting 3D set of fibres and contact regions are given in Figure 2e and 2f. From Figure 2f, we are able to label and count the total number of detected potential contacts, which we

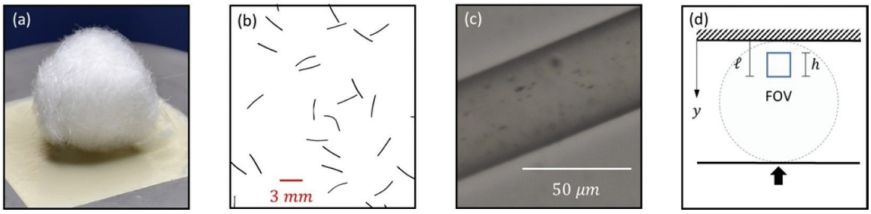

Figure 1. (a) Photograph of a nylon floc fastened to the bottom platen of the compression cell using double-sided tape. The floc in this image has a diameter of approximately 11 mm. (b) Binarized image of the length of the the individual fibres in the floc acquired from an Epson V600 flatbed scanner at 10 μm pixel size. (c) Light micrograph of a portion of a single fibre, acquired using an optical microscope with a 40x lens. (d) Schematic of the location of the field of view (FOV) relative to the stationary upper platen. For all cases h = 2 mm and l = 1.4 mm.

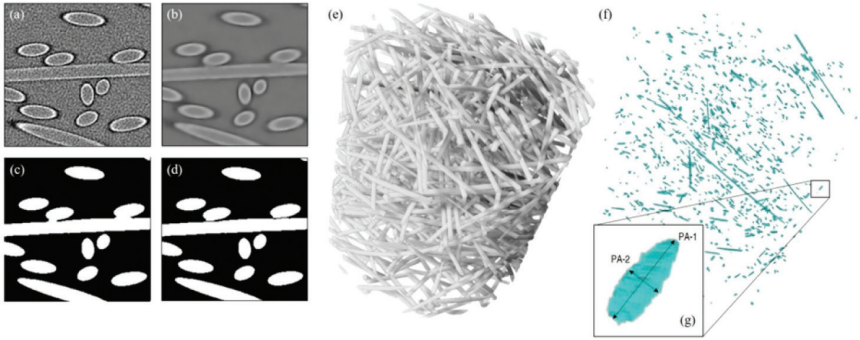

Figure 2. This sequence of images highlights the image polishing pipeline. In the first four steps, we demonstrate the image processing operation on the same slice from the z-stack. (a) The raw image highlighting noise and beam hardening on the individual nylon fibre grains. The eccentricity of the cross -sectional area results from orientation of the particle relative to the beam direction. (b) Filtering using 3D anisotropic diffusion algorithm. (c) Binarized image with with white nylon fibres (255) and a black background (0). Of note are the two contact points formed along the central horizontal fibre. These will be captured in the next step where we segment the individual particles. (d) The watershed segmentation method is applied on the 3D Euclidean Distance Map of the binary image and provides separated objects from which contact regions are extracted. (f) 3D rendering of the scanned window of the uncompressed floc. (f) 3D rendering of the contact regions in the corresponding uncompressed floc. (g) Zoom in on a typical ellipsoidal contact region between two cylindrical particles whose shape (and Principal Axis PA) depend on the relative orientation of the particle.

define as n_d. We attempt to segment the true from the false contacts in n_d using the methodology advanced by Sibellas et al. In this previous work, we studied contact in systems of mono- and polydisperse spherical grains. We identified that a disc-like object is formed when each contact-volume, having the shape of an ellipsoid, is projected onto a plane normal to the line connecting the two centres of the spheres. This disclike object can be characterized by two principle axis (PA) referred as PA_1 and PA_2 (see Figure 2g). Utilizing unique calibration experiments, we observed that the ratio of $PA_1/PA_2 \approx 1$ and that PA_1 decreased with increasing centreto-centre distance. We reported that the radii of true contacts was clustered around a central mean that is statistically larger than that of the false contacts. In addition, we reported the true contact population to be Gaussian-distributed and advanced a clustering algorithm, similar to an expected maximisation segmentation, to segment true contacts from false. Key to developing this methodology was knowledge of the population distribution of the contact radii R_c, formed by assigning $R_c \approx PA_1$ for each individual contact.

Although the systems we describe in the present work are different to that reported in our previous study, we use this technique cautiously through use of an assumption. For the special case of a large aspect ratio circular rod, where the radius of curvature along its length is significantly greater than the cross-sectional radius, the imaged contact surface forms an ellipse. In this limit, the magnitude of the major axis (PA_1) is related *primarily* to the crossing angle. Crucially, the magnitude of the minor axis (PA_2) is only *weakly* dependent on the crossing angle (as the radii of curvature of the diameter is vastly different than that along its length). With this, we use our previous methodology to identify contacts directly by assuming that

$$R_c = min(PA_1, PA_2) \tag{1}$$

This assumption yields an estimate of the true number of contacts. Finally, we estimate ρ_c by normalizing the number of contacts by the volume of our image. We report both upper and lower bounds for ρ_c, with the upper bound estimated by n_d and the lower bound using our contact identification methodology for mono- and polydisperse spherical grains.

3 RESULTS AND DISCUSSION

In this section we present the results of this imaging campaign. We start by presenting the force-displacement curves in conjunction with a library of 3D images from the lab frame of reference. We complement this by changing the

frame of reference and present the trajectory of one individual fibre during compression. Finally, we present estimates of the evolution of ρ_c.

We begin by examining the force-displacement curve shown in Figure 3. Two curves are displayed: a solid black line representing a continuous deformation result and a blue line representing an interrupted deformation curve where systematic holds were programmed in order to acquire an image. The imaging points are also labelled in the figure, beginning with the initial undeformed state (S_0) and ending after 6 mm of deformation (S_6). The first observation that can be made is that during continuous compression, the load F increases monotonically with displacement D and describes a power-law behavior commonly reported for the slow compaction of granular materials. In contrast, with interrupted loading, superposition of two experimental results occurs at small displacement, followed by stress relaxation during the hold periods at larger displacements >4 mm. Similar phenomena have been observed with papermaking fibre suspensions [21].

Figure 4 presents a library of images of the evolution of floc architecture as a function of the degree of compression to help gain insight into the observed phenomena. Qualitatively we observe the orientation evolving from a "random-like" structure initially to more of a planar-structure with increasing compression. We also note that if we track an individual fibre (see Figure 5), the fibre starts slightly curved but then straightens and becomes wavy with increasing compression. We also observe densification occurs by sliding and rotation in the early stages of compression (see Figure 4).

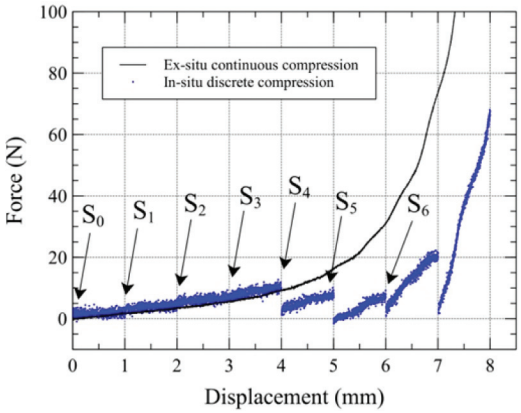

Figure 3. The force-displacement curve of the experiment is reported in blue dots. The beginning of the curve follows the same trend as the force-displacement curve obtained on a similar flock with a continuous compression. Stopping the compression to perform the tomograph scans allows the sample to relax which makes the compression force drop. The scans are launched once the force relaxation has stabilized (not reported on the graph).

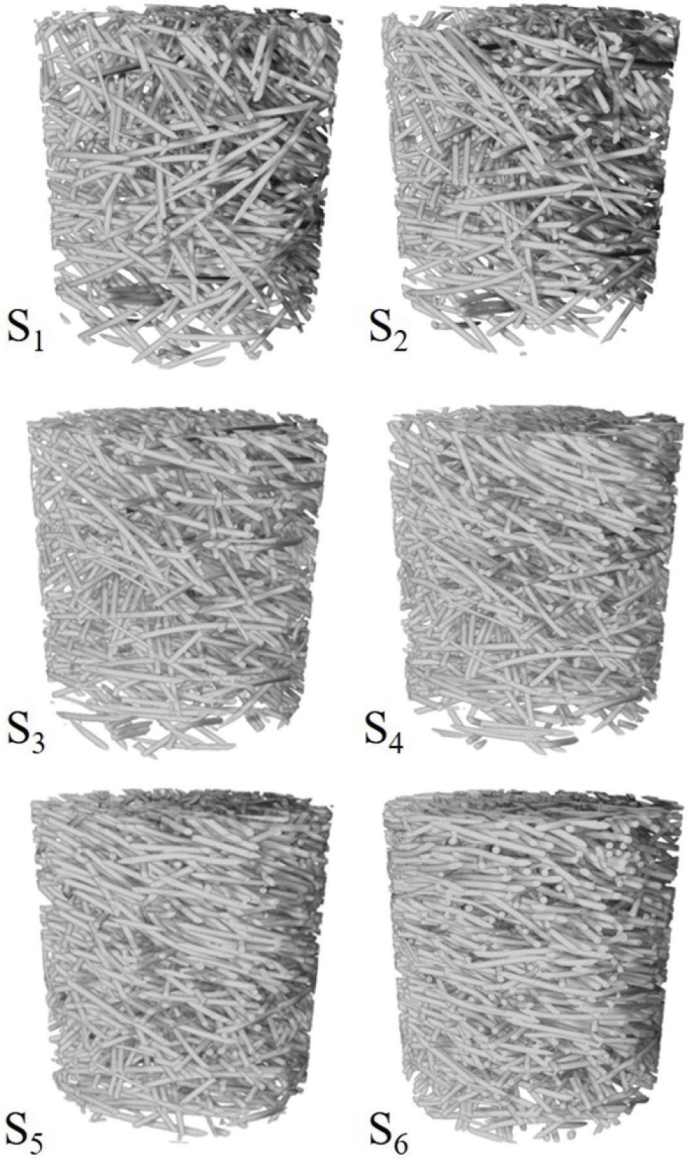

Figure 4. 3D rendered images are reported from S_1 to S_6. The compaction of the structure is clearly observed as well as fibre reorientation and fibre bending.

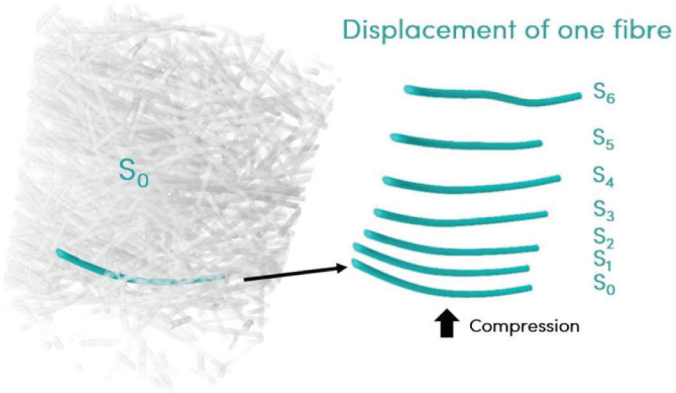

Figure 5. One nylon fibre (in cyan) from the initial scan S_0 is tracked through the steps of compression. This initially curled fibre follows a translation and a rotation as it reaches contact points that make it wavy.

Finally, Figure 6 presents our estimate of the density of contacts for each step of nylon fibre floc compression as a function of the fibre volume fraction φ. The blue diamonds correspond to the density of true contacts, the green triangles represent the density of the total detected contacts (true and false contacts), and φ has been determined from the X-ray tomography datasets. As can be seen, the number of false contacts is generally about 20–25%. For comparison purposes, the contact density predicted by the Random Contact Model (RCM) derived for high-aspect ratio fibres [22], as well as Toll's theoretical curve for 2D random fibres [23] are also depicted in the figure. The RCM predictive curve is surrounded by a gray area which represents a variation of 5% of the fibre diameter in the model.

In comparing these three curves, it can be seen that both the RCM approach and Toll's curve both over-estimate the density of contacts as compared to the experimental measurements, with Toll's curve showing much larger values. Effectively, the RCM predicts that $\rho_c \propto \varphi^2$. Our data does not support this functional form. We are uncertain as to the discrepancy between the theory and the model for initial values of ρ_c. One particularly troubling fact is that the experimental conditions can not match the assumptions used to develop the theory, i.e., frictionless, randomly distributed rigid straight particles. We question the role of interparticle friction, which is avoided in the present model. Song et al. [16] for example, argues that friction plays an important role on the coordination number, i.e., the density of contacts of the assembly. Highest coordination numbers are

obtained (analytically and numerically) for frictionless particles whereas they are reduced with an increase in the friction coefficient. Therefore, the friction the experimental conditions cannot match the assumptions used to develop the theory, i.e., frictionless, randomly distributed rigid straight particles. We question the role of interparticle friction, which is avoided in the present model. Song et al. [16] for example, argues that friction plays an important role on the coordination number, i.e., the density of contacts of the assembly. Highest coordination numbers are obtained (analytically and numerically) for frictionless particles whereas they are reduced with an increase in the friction coefficient. Therefore, the friction that exists between nylon fibres could be a first explanation of the observed discrepancy between theoretical and experimental values. Larger deviations at higher fibre volume fraction ($\varphi = 0.21$) can be explained by the increased curvature of the fibres due to their bending. The prediction of the density of contact for this state of the structure goes beyond the RCM theoretical framework. Notably, the evolution of ρ_c as a function of the floc compression strain ε_c (defined as $l–l_0/l_0$ with l_0 and l being respectively the initial and updated distance between compression platens) follows an equation of the form:

$$\Delta\rho_c = \rho_c - \rho^o{}_c = a\varepsilon^3{}_c \tag{2}$$

where the fitting parameters are shown in Figure 6b.

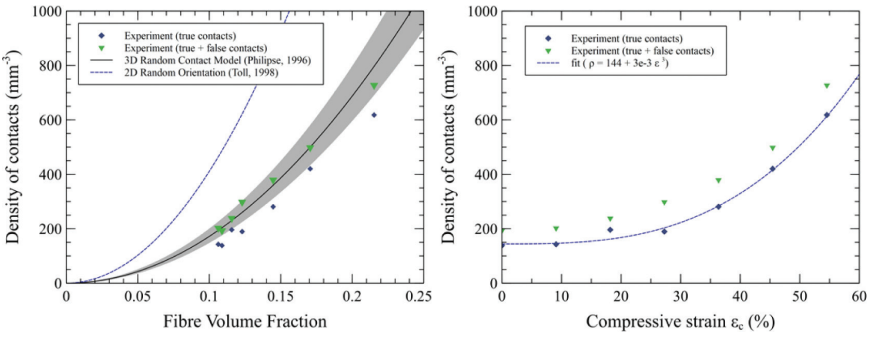

Figure 6. (a) Comparison between the experimental density of contact and the Random Contact Model [22] for 3D random straight rigid rods. The predicted curve for a 2D structure from Toll's model [23]. (b) Density of contacts ρ_c versus the compression strain ε_c of the floc.

4 SUMMARY AND CONCLUSION

In this work, we have visualized the architecture of an isolated nylon fibre floc using X-ray computed tomography. Imaging proceeded step-wise, cycling between compression and hold periods, where we acquired the images. The grains of the floc were composed of monodispersed large aspect ratio flexible cylinders (l/d = 80). Images, obtained using a Zeiss Xradia Versa 520, were first filtered with an edge-preserving algorithm and then binarized. Segmentation and labelling were carried out with a 3D marker-controlled watershed algorithm seeded by the extended-maximas of a 3D Euclidian Distance Map. In total, 7 steps of compression were collected were we created a library of 3D rendered architectures with corresponding load and solid volume fractions. In the early stages of compression, we note densification through sliding and rotation. At later stages, we observed that fibres, which were initially (slightly) curved, straightened and then became wavy under the action of their nearest neighbours. We quantified our images and placed bounds on the estimate of $\rho_c(\varphi)$ which is overestimated by the Random Contact Model. We suspect the role of friction between particles which is not included in the theory. Morevover, we advance that $\rho_c \propto \varepsilon_c^3$.

REFERENCES

[1] W. J. Batchelor, J. He and W. W. Sampson, Inter-fibre contacts in random fibrous materials: experimental verification of theoretical dependence on porosity and fibre width, *Journal of Materials Science* 41 (24) (2006) 8377–8381. doi:10.1007/pl00021935. URL https://doi.org/10.1007/PL00021935

[2] X. Thibault and J. F. Bloch, Structural analysis by X-ray microtomography of a strained nonwoven papermaker felt, *Textile Research Journal* 72 (6) (2002) 480–485. doi:10.1177/004051750207200603.

[3] W. O. Smith, P. D. Footem and P. F. Busang, Packing of homogeneous spheres, *Physical Review* 34 (9) (1929) 1271–1274. doi:10.1103/PhysRev.34.1271. URL https://link.aps.org/doi/10.1103/PhysRev.34.1271

[4] J. D. Bernal, J. Mason, Packing of spheres: Co-ordination of randomly packed spheres, *Nature* 188 (4754) (1960) 910–911. doi:10.1038/188910a0.

[5] M. Arakawa and M. Nishino, Contact Number and Porosity in Randomly Packed Sphere Mixtures of Various Sizes, *Journal of the Society of Materials Science, Japan* 22 (238) (1973) 658–662. doi:10.2472/jsms.22.658.

[6] D. Pinson, R. P. Zou, A. B. Yu, P. Zulli and M. J. McCarthy, Coordination number of binary mixtures of spheres, *Journal of Physics D: Applied Physics* 31 (4) (1998) 457–462. doi:10.1088/0022-3727/31/4/016. URL https://doi.org/10.1088/0022-3727/31/4/016

[7] R. P. Zou, X. Bian, D. Pinson, R. Y. Yang, A. B. Yu and P. Zulli, Coordination number of ternary mixtures of spheres, *Particle and Particle Systems Characterization* 20 (5) (2003) 335–341. doi:10.1002/ppsc.200390040.

[8] A. Donev, I. Cisse, D. Sachs, E. A. Variano, F. H. Stillinger, R. Connelly, S. Torquato and P. M. Chaikin, Improving the Density of Jammed Disordered Packings Using Ellipsoids, *Science* 303 (5660) (2004) 990–993. doi:10.1126/science.1093010.

[9] J. Blouwolff and S. Fraden, The coordination number of granular cylinders, *Europhysics Letters* 76 (6) (2006) 1095–1101. doi:10.1209/epl/i2006-10376-1. URL https://doi.org/10.1209/epl/i2006-10376-1

[10] M. Wiebicke, E. Ando, I. Herle and G. Viggiani, On the metrology of interparticle contacts in sand from x-ray tomography images, *Measurement Science and Technology* 28 (12) (2017) 124007. doi:10.1088/1361-6501/aa8dbf.

[11] T. Aste, M. Saadatfar and T. J. Senden, Geometrical structure of disordered sphere packings, *Physical Review E – Statistical, Nonlinear, and Soft Matter Physics* 71 (6) (2005) 61302. arXiv:0502016, doi:10.1103/PhysRevE.71.061302. URL https://link.aps.org/doi/10.1103/PhysRevE.71.061302

[12] F. M. Schaller, M. Neudecker, M. Saadatfar, G. Delaney, K. Mecke, G. E. Schröder-Turk, and. Schröter, Tomographic analysis of jammed ellipsoid packings, *AIP Conference Proceedings* 1542 (1) (2013) 377–380. doi:10.1063/1.4811946. URL https://aip.scitation.org/doi/abs/10.1063/1.4811946

[13] Y. Fu, Y. Xi, Y. Cao and Y. Wang, X-ray microtomography study of the compaction process of rods under tapping, *Physical Review E – Statistical, Nonlinear, and Soft Matter Physics* 85 (5) (2012) 2–9. doi:10.1103/PhysRevE.85.051311.

[14] X. D. Zhang, C. J. Xia, X. H. Xiao and Y. J. Wang, Fast synchrotron X-ray tomography study of the packing structures of rods with different aspect ratios, *Chinese Physics* B 23 (4) (2014) 44501. doi:10.1088/1674-1056/23/4/044501.

[15] G. W. Delaney, T. Di Matteo and T. Aste, Combining tomographic imaging and DEM simulations to investigate the structure of experimental sphere packings, *Soft Matter* 6 (13) (2010) 2992–3006. doi:10.1039/b927490a. URL http://dx.doi.org/10.1039/B927490A

[16] C. Song, P. Wang and H. A. Makse, A phase diagram for jammed matter, *Nature* 453 (7195) (2008) 629–632. doi:10.1038/nature06981.

[17] EMPA Materials Science and Technology, Xlib (Fiji Plugin). URL http://wiki.imagej.net/Xlib

[18] D. Tschumperlé and R. Deriche, Vector-valued image regularization with PDE's: A common framework for different applications, *Proceedings of the IEEE Computer Society Conference on Computer Vision and Pattern Recognition* 1 (4) (2003) 506–517. doi:10.1109/cvpr.2003.1211415.

[19] L. Vincent, L. Vincent and P. Soille, Watersheds in Digital Spaces: An Efficient Algorithm Based on Immersion Simulations, *IEEE Transactions on Pattern Analysis and Machine Intelligence* 13 (6) (1991) 583–598. doi:10.1109/34.87344.

[20] J. Ollion, J. Cochennec, F. Loll, C. Escudé and T. Boudier, TANGO: A generic tool for high-throughput 3D image analysis for studying nuclear organization, *Bioinformatics* 29 (14) (2013) 1840–1841. doi:10.1093/bioinformatics/btt276. URL https://doi.org/10.1093/bioinformatics/btt276

[21] R. J. Kerekes, Rhology of fibre suspensions in papermaking: An overview of recent research, *Nordic Pulp and Paper Research Journal* 21 (5) (2006) 598–612. doi:10.3183/npprj-2006-21-05-p598-612.URLhttps://doi.org/10.3183/npprj-2006-21-05-p598-612

[22] A. P. Philipse, The Random Contact Equation and Its Implications for (Colloidal) Rods in Packings, Suspensions, and Anisotropic Powders, *Langmuir* 12 (24) (1996) 5971–5971. doi:10.1021/la960869o.

[23] S. Toll, Packing mechanics of fiber reinforcements, *Polymer Engineering and Science* 38 (8) (1998) 1337–1350. doi:10.1002/pen.10304.

VISUALISATION OF THE 3D MICROSTRUCTURE OF A MONODISPERSE FIBRE ASSEMBLY UNDER UNIAXIAL COMPRESSION

A. Sibellas[1], *J.E.Q.M. Litjens*[1], *J. Drummond*[1], *A.B. Phillion*[2] *and D.M. Martinez*[1]

[1] Department of Chemical and Biological Engineering, The University of British Columbia, Vancouver, Canada
[2] Department of Materials Science and Engineering, McMaster University, Hamilton, Canada

Steven Keller Miami University

You did not fully address the segmentation process that you used. My question is that if you modified the segmentation process, would the position or the width of contact distributions change? It seems that you are assuming that a certain segmentation process provides a specific measured contact area between the spheres. Secondly, you have taken physical spheres and converted them to discrete voxels in Cartesian space in the tomographic imaging process. Could that account for the secondary false distribution, which we are seeing or add to the width of the primary distribution?

Aurelian Sibellas

For the first part, the segmentation will change the overall distribution. What I have not shown here is that if you change the filtering for the binarisation in the segmentation you will shift your Gaussian distribution, but the good thing about the method is that you will still extract the correct number of contacts. You will just change the number of false contacts.

Discussion

Steven Keller

And of course when comparing the Cartesian to the actual spherical coordinate because if you take a look at your pictures, you can actually see in your images that if contact is made in the 2 o'clock position on the sphere then it will create a different contact area than if you make contact where the spherical surface intersects the principal Cartesian axes such as the 12 o'clock or 9 o'clock positions.

Aurelian Sibellas

It is hard to tell, the thing is the discs are the contacts so to find the contact radius it assumes that it is a perfect circle. So, we use an equivalent contact radius and it will depend on the orientation. I do not think it will have a huge effect since our discs have usually the size of a dozen voxels. It depends on the orientation, but I do not think it plays a huge role in ours.

Jukka Ketoja VTT Technical Research Centre of Finland Ltd

I found your nylon fibre sample very interesting as it could help us to understand what goes on in the lightweight wood fibre materials, for instance. So, I was not quite sure whether your fibres are bonded together somehow or they are able to slide frictionally?

Aurelian Sibellas

No, they are not tested frictionally. I do not know what the coefficient of friction is. They are not bonded together. They are just making random structures. We have not characterised the interaction between the fibres. We really focused on the structure.

Jukka Ketoja

There is a lot of theoretical work about wool for instance where the fibres can slide. Have you looked at how the stress develops during compression and combined that, for instance, with the increase in the fibre contacts?

Aurelian Sibellas

We have not correlated the force and we have not looked at the mechanics of the floc. We only focused on the number of contacts. I know there are mechanical models that are built on the 3D estimation of contacts and it would be certainly

interesting. My goal was to be able to extract the contacts, so I did not spend much time on the mechanics of the floc.

Jukka Ketoja

Anyway, I think your work lays a good foundation for further development of the analysis of mechanical properties.

Bill Sampson University of Manchester

It is very nice to see the progress in this work since we spoke about a year ago. I have a couple of comments and a question. The first comment is about something you said towards the end of your talk concerning the curvature of fibres as the cause of the discrepancy between your measurements and the models. This will not be the case. If you think of a network of straight fibres and then you take one fibre and bend it, then the probability that you will make a new contact is the same as the probability that you will break an existing contact. So, actually the curvature of fibres in true 3D random structures has no effect on the instance of contact.

Aurelian Sibellas

So, my comment on the discrepancy at the end is not valid about the bending.

Bill Sampson

No. But the thing that does matter, and I think cause of the main departure of the data from the model, is that you are inducing a non-randomness because you no longer have 3D random orientation; you put a bias in.

And now for my question. Have you looked at the distribution of the ratio of the minor to major axes of your ellipse on your nylon fibres? That will give you the sine of the angle of contact between the fibres?

Aurelian Sibellas

You are totally right. I have not looked at this although it is coded because I have checked for the spheres and this ratio, so I told you for the spheres I talked about an equivalent contact radius because it is not perfectly circular. So, I know I can have this ratio. I have not checked it between the fibres. It would be very interesting. It would surely give us another perspective on the orientation between the fibres, I have not done it.

Discussion

Bill Sampson

I think it is really nice because it will provide a measure of how far away you have moved from the pure random case that is considered in the theories.

Shubham Agarwal University of British Columbia

I have a question from the very last slide in which you have shown an equation, so does this equation come from a model or is it a fit?

Aurelian Sibellas

Oh yes, it is a very nice article from Stefan Toll in 1998. Basically, it is the contact density in a 3D random structure of rod-shaped particle.

Shubham Agarwal

Because what I believe is that there should be a threshold volume fraction below which the density of contact will be zero, since below a certain volume fraction there will be no contact as fibres will be well-separated. However the equation doesn't show any such evidence.

Aurelian Sibellas

I think the model is for high aspect ratio fibres. This is what I forget to mention.

Jee-Hong Lee Seoul National University

I have two questions. First question is that, if I understood your right, you made a model study with the spheres and moved on to the experiment using the nylon rods. Just a simple concern or question is that there might be some difference if you use the rod-shaped models to establish the things such as calibration principle or something like that. So, have you ever tried using rod-shaped models to establish or will there be any problems that may happen if you use the spheres instead of that.

Aurelian Sibellas

So, what I have done before the nylon fibres is I studied contacts between structures made of spaghetti and nails and we had a problem. The method works for high aspect ratio particles because I do not want the end to end contact. But with

nails and spaghettis, if you want a high aspect ratio, you will have very very long spaghetti. I doubt that Barilla is making such pasta so we could not use that. And you have a wall effect from the container, so maybe you will have very high aspect ratio of particles, but your container has to be at least 5 or 10 times the size of the longest axis, so it becomes impossible to study with tomography. So, this is why we used the nylon fibres because you have very high aspect ratio particles. Was this your question?

Jee-Hong Lee

Yes. The second one is that you are ultimately aiming for the application to some very complex network structures like paper, and you know there are lots of paper products whose components are ranging from nano size to the micro size, and even to the macro size. The imaging is always a kind of competition between the resolution and the size. I am not sure that how much the X-ray will show an adequate resolution for the products containing nano sized particles. So, what kind of applications are you having in mind?

Aurelian Sibellas

So basically I have developed these to better understand the contacts that we have in paper handsheets. You said about the resolution.

Jee-Hong Lee

Yes. The resolution – and also if the imaging method can detect a wide range of particles including small fines, cellulose nanofibrils, and macro fibres. Researchers have even tried to put cellulose nanofibres into papermaking.

Aurelian Sibellas

Basically, you choose your resolution, which has a function of the smallest feature you want to measure, so here in paper handsheets it's often the fibre wall thickness, and let's say we want 5 or 10 pixels to describe those thicknesses and it will tell you the resolution. So, the images we have so far are 1 or 2 micron in resolution. I do not think it is enough to really get the curvatures of the fibre to reach the true number of contacts, although we could reach to contact surfaces, but this might not be enough to really know if it is a contact. So, I think for such a structure it would be better to be at a higher resolution.

Discussion

Anton Hagman RISE Research Institutes of Sweden

On this slide, the fibre volume fraction is mentioned, I guess that you have calculated from the picture what is fibres and not. Have you looked at the distribution, especially some sections seem to differ and are not even all over. Do you compensate for this in some way and can this have something to do with the shift you see in the graph?

Aurelian Sibellas

I am sorry, the distribution . . .?

Anton Hagman

I think if go back a couple of slides where you have the sections. If you look at S4 and you look in the top corner, you see that it is much denser up there than it is down in the centre. So, have you used some kind of mean value for the whole field of view?

Aurelian Sibellas

You're right. It is relevant. We have an uneven density of fibres through the vertical axis. I think the window here is quite small, so we used an average estimation of the contacts although I could discretise but I needed a lot of contacts to be able to have good average. But yes there is a slight difference in the number of contacts between the top and bottom.

Anton Hagman

Something I noticed and wonder how you had done it, really good work.